# Breath hold effect on cardiovascular brain pulsations – A multimodal magnetic resonance encephalography study

Lauri Raitamaa[1] ⓘ, Vesa Korhonen[1,2], Niko Huotari[1],
Ville Raatikainen[1], Taneli Hautaniemi[1], Janne Kananen[1] ⓘ,
Aleksi Rasila[1], Heta Helakari[1], Aleksandra Zienkiewicz[3],
Teemu Myllylä[1,3], Viola Borchardt[1] and Vesa Kiviniemi[1,2]

## Abstract

Ultra-fast functional magnetic resonance encephalography (MREG) enables separate assessment of cardiovascular, respiratory, and vasomotor waves from brain pulsations without temporal aliasing. We examined effects of breath hold- (BH) related changes on cardiovascular brain pulsations using MREG to study the physiological nature of cerebrovascular reactivity. We used alternating 32 s BH and 88 s resting normoventilation (NV) to change brain pulsations during MREG combined with simultaneously measured respiration, continuous non-invasive blood pressure, and cortical near-infrared spectroscopy (NIRS) in healthy volunteers. Changes in classical resting-state network BOLD-like signal and cortical blood oxygenation were reproduced based on MREG and NIRS signals. Cardiovascular pulsation amplitudes of MREG signal from anterior cerebral artery, oxygenated hemoglobin concentration in frontal cortex, and blood pressure decreased after BH. MREG cardiovascular pulse amplitudes in cortical areas and sagittal sinus increased, while cerebrospinal fluid and white matter remained unchanged. Respiratory centers in the brainstem – hypothalamus – thalamus – amygdala network showed strongest increases in cardiovascular pulsation amplitude. The spatial propagation of averaged cardiovascular impulses altered as a function of successive BH runs. The spread of cardiovascular pulse cycles exhibited a decreasing spatial similarity over time. MREG portrayed spatiotemporally accurate respiratory network activity and cardiovascular pulsation dynamics related to BH challenges at an unpreceded high temporal resolution.

## Keywords

Breath hold, cardiovascular pulsations, cerebrovascular reactivity, magnetic resonance encephalography, respiratory centers

Received 22 March 2018; Accepted 29 July 2018

## Introduction

In early years of functional magnetic resonance imaging (fMRI), physiological pulsations were regarded as noise that obscures hemodynamic responses coupled to neuronal activity in blood oxygen level-dependent (BOLD) signals. In 1995, Biswal et al.[1] detected functionally connected low frequency fluctuations <0.1 Hz in the resting-state BOLD signal. Since then, fluctuation patterns have been intensely studied with the aim to quantify fundamental properties of spontaneous human brain activity.

Despite the advancement in imaging quality, preprocessing and modeling methods, interactions between

[1]Oulu Functional Neuro Imaging Group, Research Unit of Medical
Imaging Physics and Technology (MIPT), University of Oulu, Oulu, Finland
[2]Department of Diagnostic Radiology, Medical Research Center (MRC),
Oulu University Hospital, Oulu, Finland
[3]Biomedical Sensors and Measurement Systems Group, Optoelectronics
and Measurement Techniques Unit, University of Oulu, Oulu, Finland
The first two authors contributed equally to this work.

**Corresponding author:**
Vesa Korhonen, Department of Diagnostic Radiology, Oulu University
Hospital, P.O. Box 50, Oulu 90029, Finland.
Email: vesa.korhonen@oulu.fi

different physiological pulsations affecting the cerebral BOLD signal remain unclear. This uncertainty in part originates from the fact that whole-brain fMRI studies usually sample brain data slowly, i.e. one brain volume is imaged every 2–3 s. At this slow image sampling rate, the cardiorespiratory signal gets aliased over low frequencies and is indistinguishable. Moreover, acquiring interleaved image slices further complicates the detection of propagating physiological signals.

Novel ultra-fast 3D k-space under-sampling techniques, like magnetic resonance encephalography (MREG), enable imaging of the whole brain within 0.1 s and impede cardiorespiratory aliasing.[2] MREG combined with synchronous cardiorespiratory monitoring can thus be used to image the temporal evolution of all physiological pulsations with whole-brain coverage.[3]

In the past, the research on cardiovascular brain pulsations has not gained much interest, as their physiological role was neither strongly tied to neuronal activity, nor to anything other than noise covering the neuronal signal. However, the recent discovery of the glymphatic brain clearance system has increased the understanding of the physiological role of cardiovascular pulsations as a driving force for maintaining brain homeostasis.[4] Recently, three glymphatic pulsation mechanisms, namely cardiovascular, respiratory, and very low frequency vasomotor waves, were found using resting-state MREG data.[3]

Cerebral blood circulation is known to be modulated by partial $CO_2$ pressure of blood and end tidal $CO_2$ ($etCO_2$). Due to the known correlation between $etCO_2$ and cerebral blood flow (CBF), respiratory challenges like breath holding (BH) and hyperventilation have been used to calibrate and quantify BOLD signals.[5–13] Fluctuations in $etCO_2$ increase temporal correlation of the BOLD signal in distant regions of grey matter due to vascular reactivity in addition to neuronal activity.[14–16]

Voluntary breath-holding globally increases the BOLD signal due to $CO_2$-induced cerebral vasodilation, whereas hypocapnia arising from hyperventilation reduces the BOLD signal.[17,18] Initially during BH, the altered ratio of oxy-/deoxygenated hemoglobin decreases the BOLD signal, whereas the subsequent compensatory vasodilation leads to both increased blood flow and volume, which increases the signal intensity above the baseline after the initial dip.[6] Specifically, oxygenated hemoglobin concentration increases during BH, while deoxygenated hemoglobin concentration remains constant, as measured with functional near-infrared spectroscopy (NIRS) placed on the forehead.[19,20]

During BH, expression of the central respiratory rhythm is not stopped but merely suppressed.[21] Long BH produces discomfort (which is not equally tolerated by all subjects) and has transient but strong boosting effects on respiration-mediated changes in heart rate (HR), which in turn can induce anxiety- and stress-related changes of the cardiovascular system.[19,22] The respiratory output is a result of a complex interaction between deeper and higher brain areas, including the bilateral network of the primary sensorimotor cortices, the basal ganglia, the thalamus, the limbic system, the cerebellum, and the brainstem.[23–26] Especially in the brainstem, pons and medulla showed a strong BOLD sensitivity to $CO_2$ stimulation.[27] Taken together, BH is a well-established paradigm to manipulate physiological respiration patterns and thus offers a robust control measure for testing the spatial and temporal sensitivity of MREG in visualizing the alterations in cardiovascular brain pulsations. As the physiological nature of the recently discovered cardiovascular pulsations in MREG signal has not yet been investigated, we set out to investigate their role by modulating $etCO_2$ in a BH study.

In this study, we utilized multimodal MREG to explore the effects of repeated BH runs on cardiovascular pulsations of the human brain, which so far have not been examined at whole brain level with a high temporal resolution of 10 Hz. We studied whether the MREG signal reveals both classical BOLD-like signal elevations and monitors cardiovascular pulsation changes. As the role of cardiovascular pulses is not fully understood, our aim was to study whether BH induces detectable modulations of cardiovascular pulsation in MREG signal. Our hypothesis was that BH-related elevation in CBF alters cardiovascular brain pulsations due to changes in vasomotor tone as a response to the BH. This study aims to contribute to the growing area of research on the human glymphatic system by exploring how respiratory manipulation of cardiovascular pulsations influences brain fluid propulsions on high temporal resolution.

## Methods

### Subjects and paradigm

A total of 13 healthy subjects (age: $32.6 \pm 9.7$, 5 females) were placed in the MRI scanner and asked to lay still and adapt their breathing according to the instructions continuously shown on screen during MR imaging. Written informed consent was obtained from each subject prior to scanning, in accordance with the Helsinki declaration (1983). The study protocol was approved by the regional Ethical Committee of Northern Ostrobothnia Hospital District in Oulu University Hospital.

The paradigm began with a 40 s normo-ventilation (NV) resting-state measurement followed by five blocks

of 32 s breath hold and 88 s of free recuperative respiration. Subjects were instructed to hold breath during the BH period and to breathe freely during respiration periods. The subjects were informed about both start and end of each BH by white text on black background displayed on a screen (Supplementary Figure 1).

## Multimodal data acquisition and processing

Subjects were scanned using Siemens 3 T SKYRA with 32-channel head coil. MREG is a 3D single shot stack of spirals sequence that under-samples k-space in order to reach 10 Hz critical sampling of physiological pulsations.[2] Scanning parameters (TR 100 ms, TE 36 ms, flip angle 5°, 3D matrix $64^3$, FOV 192 mm) allowed a whole brain sampling rate of 10 Hz with voxel size approximately $3 \times 3 \times 3$ mm$^3$. The raw MREG data were reconstructed using Matlab *recon* tool with L2-Tikhonov regularization parameter lambda = 0.1 and the latter regularization parameter determined by the L-curve method with effective spatial resolution was 4.5 mm.[29] Anatomical 3D MPRAGE (TR 1900 ms, TE 2.49 ms, TI 900 ms, flip angle 9°, FOV 240 mm, 0.9 mm cubic voxel) images were used to register the MREG data into Montreal Neurologic Institute (MNI) space.

We used a multimodal setup as described in Korhonen et al.[28] Cardiorespiratory signals were collected using both MRI-compatible GE Datex-Ohmeda$^{TM}$ Aestiva/5 anesthesia monitor (sampling rate 300 Hz) via fingertip plethysmography (PPG) and nasal cannula (etCO$_2$, O$_2$) as well as Siemens MRI-scanner PPG and respiration belt (sampling rate 400 Hz). These datasets were recorded to verify task compliance (Figure 1(a) and (b)). During quality control, BH runs where the subject was inhaling or exhaling were excluded. In addition, data with insufficient quality (containing motion or other artifacts) were excluded. The sample sizes were MREG: $n = 11$, 44 good BHs; NIRS: $n = 10$, 39 good BHs; plethysmography/CO$_2$: $n = 8$, 31 good BHs; NIBP: $n = 10$, 39 good BHs (Supplementary Table 1).

After transformation to frequency space, Aestiva PPG signals were evaluated visually and subject-specific peaks in the cardiac band in the range of 0.8–1.65 Hz were detected. The individual peaks of the cardiac band had a mean $1.09 \pm 0.13$ Hz. Frequencies were verified by repeating the process using both the scanner PPG data and MREG data analyzed with AFNI *3dperiodogram*. All three variants of the derived cardiac frequency bands were cross-checked for correspondence and matched.
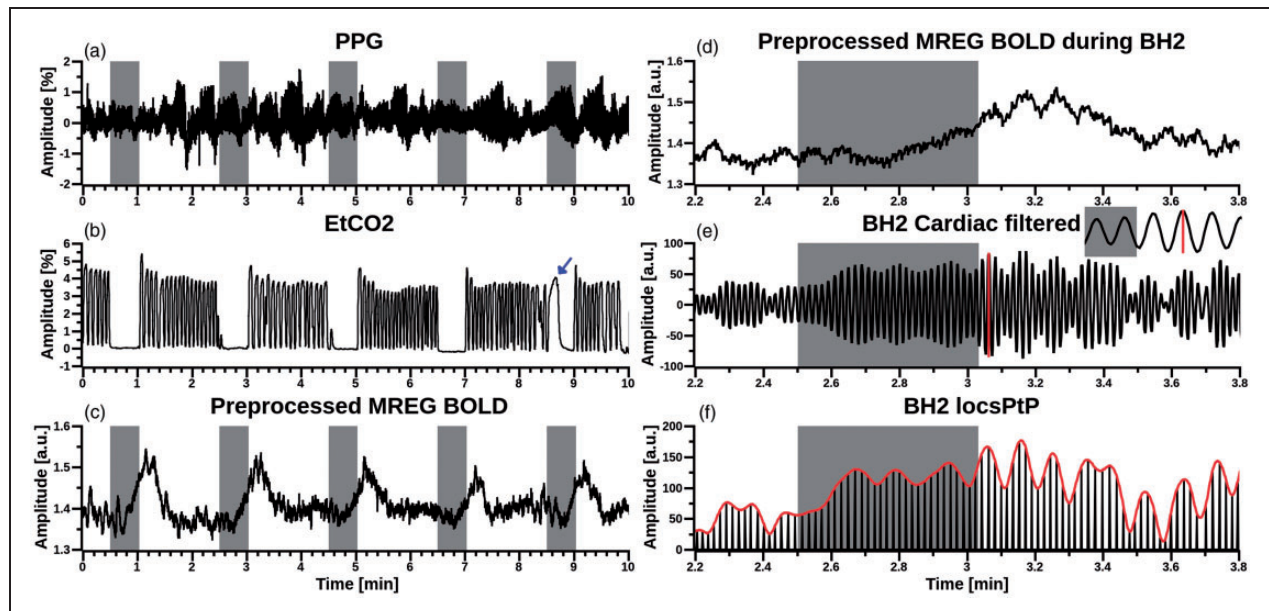


**Figure 1.** Multimodal data from one arbitrarily selected subject, with grey bars indicating subsequent BHs. (a) Aestiva/5 continuous fingertip PPG pulsations, (b) Aestiva/5 monitor etCO$_2$ signal for respiration from nasal cannula. For this subject, BH5 was excluded due to spontaneous inhalation (marked with blue arrow). (c) Amplitude of preprocessed MREG BOLD signal from anterior cingulate cortex (x = −6 mm, y = 39 mm, z = 0 mm, 4 mm spherical ROI in MNI space). (d) Magnified view of preprocessed MREG BOLD signal during BH2. (e) Band-pass filtered cardiovascular MREG signal during BH2. Inlay depicts a single pulse amplitude peak-to-peak (red vertical line) calculation. (f) Red envelope curve of cardiovascular pulse amplitude peak to peak (PtP) signal derived from (e).

Continuous non-invasive blood pressure (NIBP) was measured using two MRI-compatible opto-mechanical accelerometers (ACM).[30] ACM sensors were placed over aortic valve and carotid artery enabling measurement of central cardiac pulse transit time (PTT). Diastolic NIBP was estimated from the PTT using a non-linear model.[31,32] The results contain normalized blood-pressure curves, without stating the BP value in mmHg, which is sufficient for tracking blood-pressure oscillations (Figure 2(e)). In addition, HR was calculated in synchrony using the ACM placed over aortic valve (Figure 2(b)).

NIRS was measured using an MRI-compatible technique.[33,34] Optodes were placed on the skin above the left eye (source-detector distance: 3 cm) to quantify cortical brain oxygenation level in the left frontobasal cortex as well as arterial pulsations in synchrony with MREG (Figure 2). A modified Beer–Lambert law implemented in HoMer2 software was used to calculate concentration changes of chromophores.[35] Therefore, raw NIRS signals were converted to total hemoglobin (HbT), oxyhemoglobin (HbO), and deoxyhemoglobin (HbR) concentrations.[35] Previously described individual cardiac bands were used to filter NIRS signals. Matlab *envelope* function was used to calculate their upper and lower envelopes and their difference resulted in the individual amplitude of cortical oxygenation (Figure 2(g) and (h)).

*MREG signal preprocessing and ICA analysis.* MREG data of each subject consisted of 6552 brain volumes and preprocessing was performed using a typical FSL pipeline[36] as previously described.[3,28] In short, first 180 timepoints (18 s) were removed to minimize T1-relaxation effects and then data were high-pass filtered (cutoff 0.008 Hz). MREG data were preprocessed with FEAT, which registered the individual functional data to the T1-weighted structural data and performed spatial smoothing using 5 mm FWHM Gaussian kernel, BET brain extraction (fractional intensity=0.25, threshold gradient=0.22, neck and bias-field correction), and MCFLIRT motion correction (Figure 1(c)).

MREG data were analyzed with FSL *Melodic PICA* (model order 40) and ICA components were used to identify resting-state networks (RSNs) and physiological signal sources (white matter, CSF, vein, and artery). The set of spatial maps from the group-average analysis was used to generate subject-specific versions of the spatial maps, and associated time series, using dual regression.[37,38] The set of subject-specific dual-regressed timeseries, one per group-level ventromedial part of the default mode network (DMNvmpf), primary visual network (V1), sagittal sinus and artery spatial map were used for classical BOLD signal analysis on BH effects (Figure 2(d)).

Amplitude changes are presented as percental changes. Anterior cerebral artery, sagittal sinus, CSF, white matter, DMNvmpf, posterior cingulate cortex part of the default mode network (DMNpcc), V1, primary somatosensory network (SM1), midbrain (including putamen, pallidum, amygdala) and brainstem were selected (Figure 3, Supplementary Figure 2) by template matching with previously identified ICA components.[39,40]

*MREG cardiovascular signal amplitude mapping.* Preprocessed MREG data were band-pass filtered using individual cardiac band (as described above) using AFNI *3dBandpass* (Figure 1(e)).

Each dataset was cut into six segments: 20 s (200 MREG timepoints) of free respiration from start of the paradigm (NV0) and five times BH segments (BH1–BH5, 100 s or 1000 MREG timepoints each) containing 20 s of pre-BH free respiration, 32 s BH, and post-BH recuperative respiration of 48 s each (NV1–5), respectively. Hereafter, BH always refers to one of the latter segments.

For every voxel, MATLAB *findpeaks* function was used to localize occurrence of peaks and troughs and peak-to-peak (PtP) amplitude was calculated by subtracting the trough value from the corresponding peak value (Figure 1(e)). This method produced 4D cardiac pulse amplitude datasets (3D brain volume × 1000 timepoints, circa 100 pulse amplitude values per voxel depending on HR). These datasets represent every pulse with one positive value. The cardiovascular pulse amplitude represents the amplitude of MREG signal change due to the propagating cardiovascular pulse at each voxel.

To analyze MREG pulse amplitude changes during BH, upper envelopes of the signals were derived for every voxel using Matlab *envelope* function (Figure 1(f)). Each cardiac pulse amplitude 4D map was normalized by transformation of every voxel's amplitude value to a z-score using mean and standard deviation (SD) calculated on the respective NV0 segment. Mean and SD were calculated using AFNI *3dTstat*. 3D cardiac pulse amplitude maps were generated by reducing each voxel's timeseries to the highest z-score.

The z-score representing $p < 0.05$ (FWE-corrected at voxel level) was determined to be $z > 5.0$ using FSL *ptoz* function implementing Gaussian Random Fields Theory for multiple comparison correction (Figure 4, Table 1). The 3D cardiac pulse amplitude maps were threshold accordingly and incorporate voxels that only show a significant increase in cardiac pulse amplitude during BH. Differences in cardiac pulsation amplitude changes between BH runs were revealed by plotting normalized z-score envelope maps for BH1-5 average over subjects (Figure 4(a)). Time courses of the
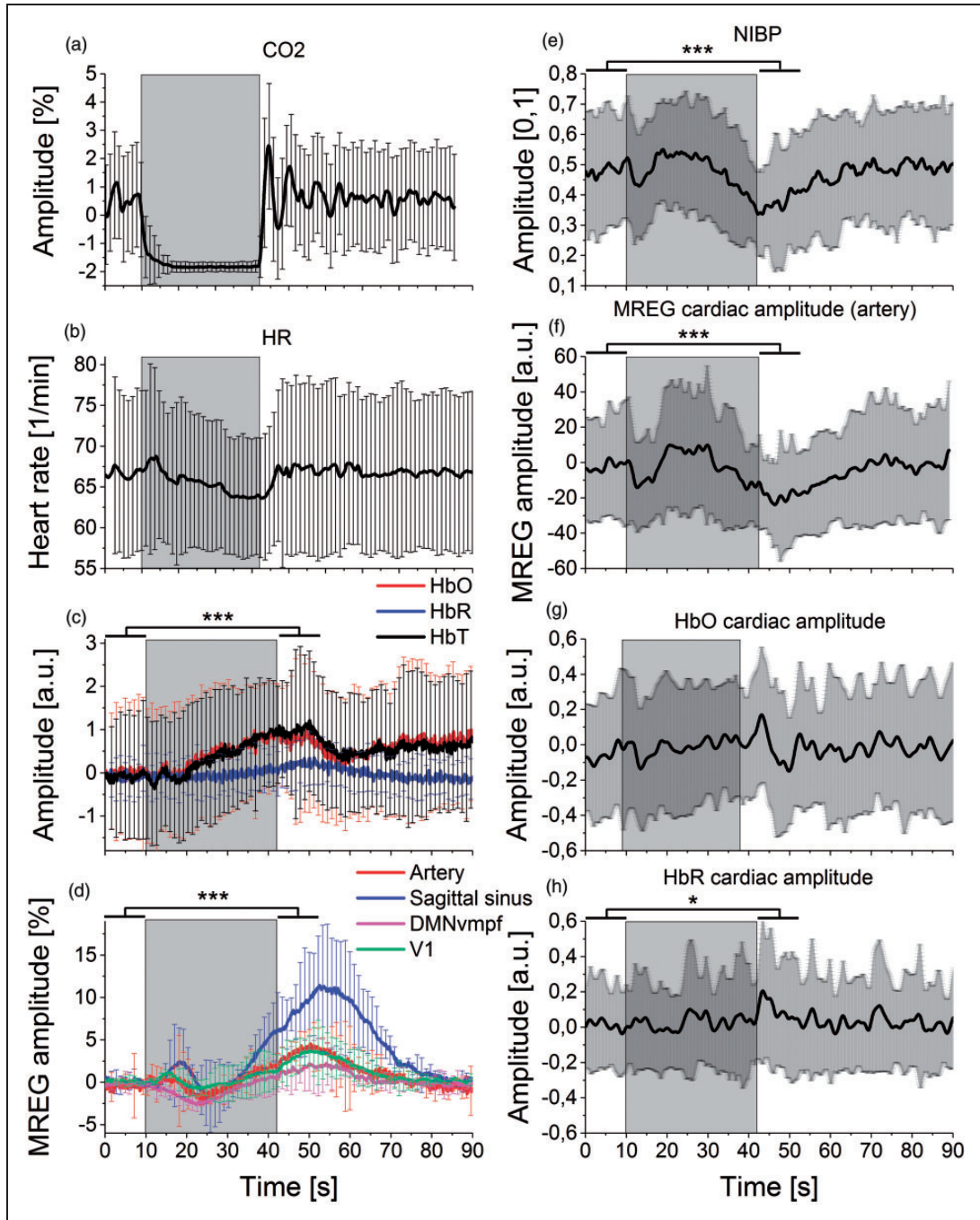
**Figure 2.** Mean signal amplitude changes during BH. The grey rectangle background marks the averaged BH period (32 s). Lines represent mean of signal amplitude and error bars represent standard deviation over subjects. Significance levels $p < 0.05*$ and $p < 0.001***$. (a) Breathing with carbon dioxide ($CO_2$), (b) heart rate (HR) from non-invasive blood pressure (NIBP) pulse data. (c) Left frontobasal NIRS measurements (fullband): oxyhemoglobin (HbO, red), deoxyhemoglobin (HbR, blue), total blood volume (HbT, black). HbO steadily increases during BH. (d) Mean MREG BOLD signals in resting-state detected using FSL Melodic PICA: anterior and both median cerebral arteries (Artery, red), sagittal sinus (blue) DMNvmpf = ventromedial part of the default mode network (magenta), primary visual network (V1, green). MREG signal amplitudes showed an initial decrease and a subsequent increase that peaked during NV after BH. (e) Continuous non-invasive blood pressure (NIBP) signal. (F) Cardiovascular pulse amplitude of MREG signal from PICA-derived IC (artery) presents two drops after the onset and end of BH. Amplitude was normalized to the first BH timepoint by subtraction. (g–h) Mean NIRS cardiovascular signal pulsation amplitudes of HbO and HbR show a modulated effect of the pressure drops seen in measures above where NIBP, MREG (artery) and HbO decrease in the early stage and after BH. Amplitudes were normalized to the first BH timepoint by subtraction.
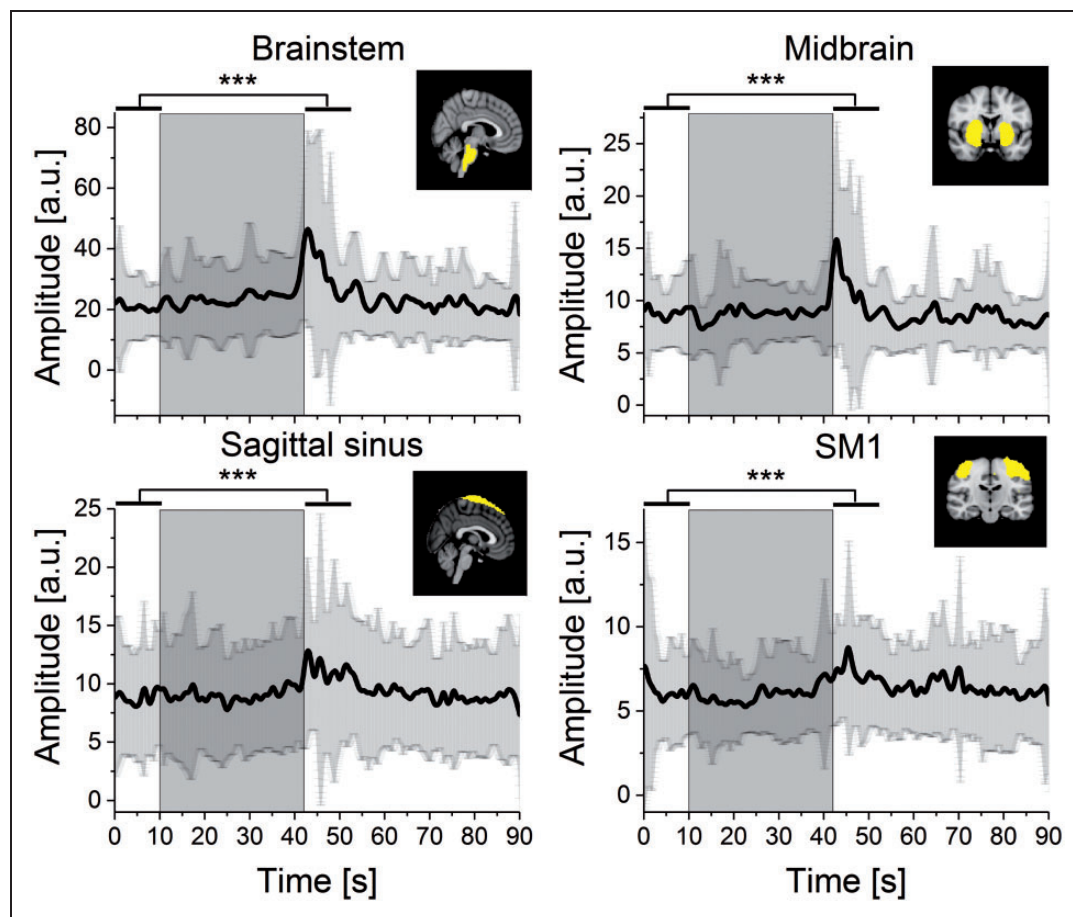
**Figure 3.** Cardiovascular pulse amplitude of MREG signal during BH from ICA-based ROIs (Sagittal sinus, primary somatosensory network (SM1), midbrain and brainstem). The grey box marks the 32 s BH period. Black lines represent mean signal amplitude and the shaded dark grey error bars represent standard deviation. All selected ROIs showed significant increases in signal amplitude following BH compared to preceding NV. Significance level after Bonferroni correction $p < 0.0056$***.

resulting significant voxels were visualized (Figure 4(a)) and their anatomical labels were derived based on the Harvard-Oxford Cortical and Subcortical Structural Atlas[41] and cross-checked with NeuroSynth (Table 1).[42] To present the general effect of cardiac pulsation amplitude changes during BH, 3D cardiac pulse amplitude maps of BH1-5 were thresholded at z > 6, binarized, and summed. The resulting image contained image values in the range of [1,3], where 3 represents a voxel that showed a significant increase in cardiac pulse amplitude in 3 of 5 BH runs (Figure 4(c)).

## Cardiovascular quasi-periodic pulse propagation analysis

We used a modified pattern finding algorithm to obtain quasi-periodic patterns (QPPs) and evaluated their changes in signal intensities and pulse propagations.[3,43]

In short, the QPP algorithm detects peaks and averages spatially similar, repeating periods of time, which in this study is the cardiac cycle of about 1 s duration depending on individual HR. The timing of the cardiovascular pulse peak was obtained from the anterior cerebral artery. Importantly, since the performance of BH showed marked individual performance variability and to be sure to capture only BH-related vasodilation in this analysis, a 22 s segment from the middle of each BH was used.

Subject-specific normalized z-scored 4D QPP map (3D × 10 timepoints representing average of cardiac pulsations) was created for each BH and NV and averaged over subjects (Supplementary Figures 4 and 5).

All average QPP maps were calculated by subtracting BH from NV (Figure 5(a)) to show how cardiac pulse spread over the brain. MATLAB circhift was used to ensure that QPP maps were on same phase and difference between NV and BH periods.
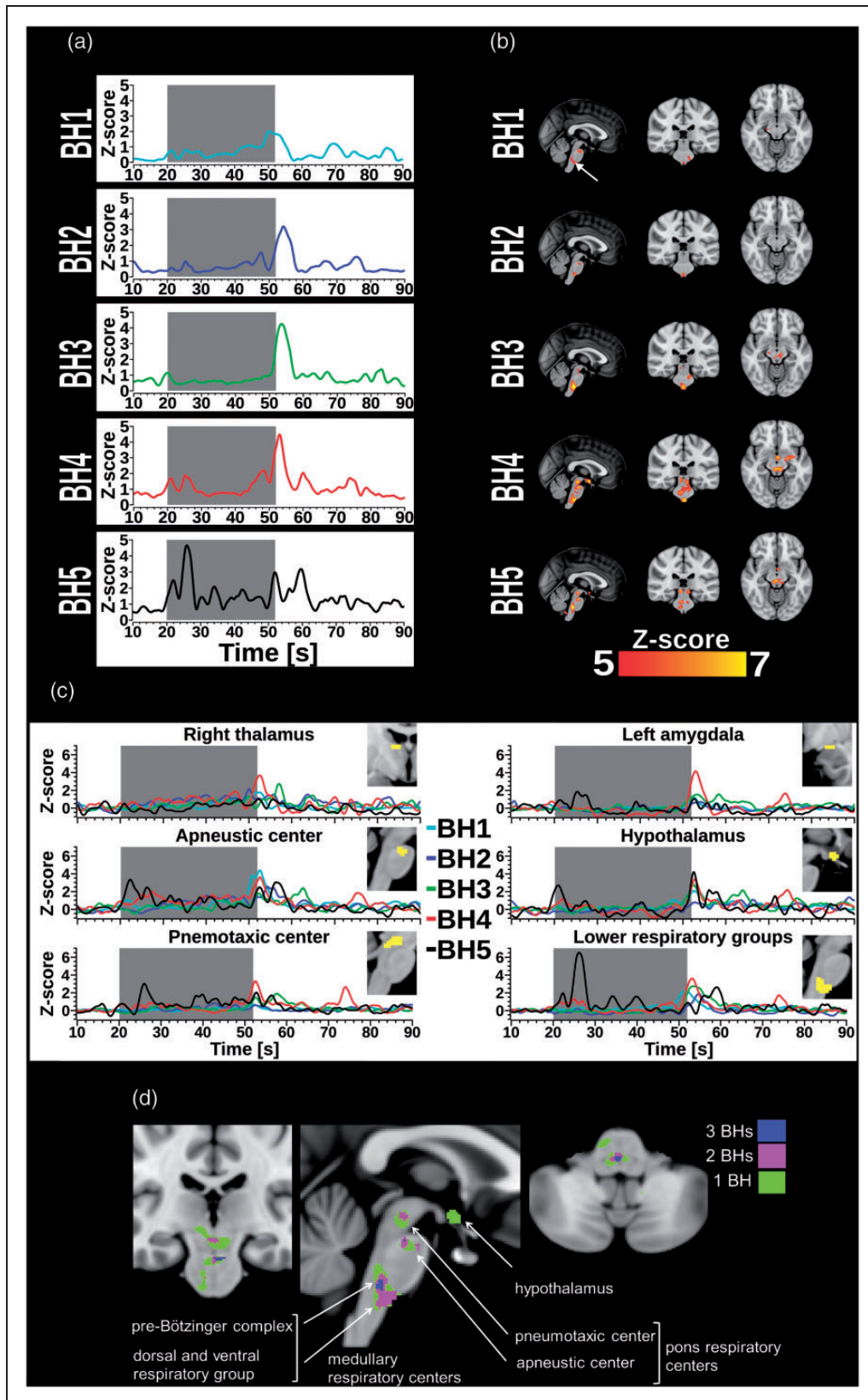
**Figure 4.** (a) For each BH run, plot shows mean time course of cardiac pulse amplitude extracted from an arbitrarily selected 4 mm spherical ROI located in lower brainstem (0, −30, −51 mm in MNI). The grey box marks the 32 s BH period. Cardiac pulse amplitude

**Table 1.** Significant results of cardiac pulse amplitude mapping.

| BH | k | z_max | X | Y | Z | Region |
|---|---|---|---|---|---|---|
| 1 | 85 | 6.5 | −4 | −24 | −24 | Left brainstem |
|  | 58 | 6 | 0 | −28 | −48 | Middle brainstem |
|  | 58 | 6.6 | −10 | −36 | −30 | Left brainstem |
|  | 34 | 5.7 | −8 | 58 | −18 | Left rectal gyrus, area fp1 |
|  | 27 | 6.1 | 18 | 0 | −20 | Right amygdala |
|  | 18 | 5.4 | 18 | −18 | −10 | Right medial geniculated nucleus |
|  | 6 | 6.2 | −18 | −10 | −24 | Left hippocampus |
| 2 | 34 | 6.2 | 0 | −30 | −48 | Middle brainstem |
|  | 32 | 6.6 | −6 | −24 | −24 | Left brainstem |
| 3 | 259 | 7.7 | 4 | −34 | −48 | Right brainstem |
|  | 126 | 6.6 | −6 | −22 | −14 | Left midbrain |
|  | 51 | 6.1 | −12 | −30 | −28 | Left brainstem |
|  | 12 | 6.1 | 12 | −4 | 12 | Right thalamus, prefrontal nucleus |
|  | 6 | 5.3 | 16 | −18 | −12 | Right midbrain |
| 4 | 948 | 7.8 | 0 | −28 | −50 | Middle lower brainstem including olivary nucleus, medial lemniscus, reticular formation |
|  | 81 | 6.6 | −18 | −6 | −12 | Left amygdala |
|  | 69 | 7.2 | 0 | −2 | −14 | Left hypothalamus |
|  | 62 | 6.6 | 10 | −4 | 12 | Right thalamus, temporal nucleus |
|  | 29 | 5.8 | 20 | −6 | −20 | Right amygdala |
|  | 29 | 5.9 | 14 | −20 | −16 | Right medial geniculated nucleus |
|  | 14 | 5.6 | −4 | −12 | 4 | Left thalamus: prefrontal nucleus |
|  | 10 | 5.3 | −38 | 12 | −24 | Left temporal pole |
| 5 | 484 | 7.5 | 0 | −36 | −40 | Middle brainstem |
|  | 189 | 7.1 | −6 | −22 | −14 | Left brainstem |
|  | 67 | 6.5 | 12 | −4 | 12 | Right thalamus, prefrontal nucleus |
|  | 36 | 6.1 | −30 | −16 | −2 | Left putamen |
|  | 22 | 6.2 | −2 | −2 | −12 | Left hypothalamus |
|  | 12 | 6.6 | 48 | −60 | −36 | Right cerebellum (crus 1) |
|  | 8 | 5.4 | 22 | −14 | 6 | Right thalamus: premotor |
|  | 7 | 6 | −36 | 6 | −30 | Left middle temporal gyrus |
|  | 6 | 5.7 | −24 | 16 | −16 | Left inferior frontal gyrus pars orbitalis |
|  | 6 | 5.3 | −36 | 16 | −28 | Left temporal pole |
|  | 6 | 5.8 | −12 | −24 | 36 | Left cerebral white matter |

Note: Significant clusters revealed by cardiac pulse amplitude mapping, sorted by BH: number of voxels in the cluster (k>5, FEW corrected on whole-brain level), maximum amplitude within the cluster (z_max), MNI coordinates [mm], and region name. BH: breath hold.

**Figure 4.** Continued
increases first manifest in the lower brainstem, but start to occur in the midbrain (thalamus, hypothalamus, and amygdala) with increasing number of BH runs. (b) Panel depicts the highest cardiac pulse amplitude maps threshold at z-score > 5 ($p < 0.05$, FWE corrected). Cardiac pulse amplitude increases first manifest in the lower brainstem, but start to occur in the midbrain (thalamus, hypothalamus, and amygdala) with increasing number of BH runs. (c) Mean cardiovascular pulse amplitudes of respiratory network ROIs (thalamus, amygdala, hypothalamus, and brainstem regions; z > 5) varied across repeated BH runs. The grey box marks the 32 s BH period. (d) General effect of repeated BH on cardiac pulse amplitudes in the respiratory centers of the brain displayed in coronal view (y = −24 mm), sagittal view (x = 0 mm), and coronal view (y = −4, in MNI). Green, magenta, and blue voxels indicate a significant z-score>6 (threshold was raised to display contoured clusters) in 1, 2, or 3 of the 5 BH runs, respectively. Labels were added in the style of Sherwood's description of respiratory centers in "Fundamentals of Human Physiology".[44]

## Statistical tests and methods

To test for differences in MREG (Figures 2(d) and (f) and 3 and Supplementary Figure 2), HR (Figure 2(b)), NIBP (Figure 2(e)), and NIRS (Figure 2(c), (g) and (h)) signal amplitudes before versus after BH, averages of 10 s before BH and 10 s after BH for each good BH were compared using a Wilcoxon signed rank test (MATLAB *signrank*) with Bonferroni correction for the respective number of multiple comparisons (significance level after Bonferroni correction for Figure 3 and Supplementary Figure 2: alpha $= 0.0056$). Equivalent $p$ and $z$-values can be found in Supplementary Table 2.

To assess spatial similarity of QPP, firstly MATLAB *corrcoef* was used to compare each BH map with the respective NV0 for every subject (Figure 5(b)). Then, correlation coefficients between BHs were compared using non-parametric two-sided paired-samples Wilcoxon signed rank test (MATLAB *signrank*, significance level after Bonferroni correction for multiple comparisons: alpha $= 0.005$, Supplementary Table 3).

## Results

### Effect of BH on exhaled CO₂, blood oxygenation, HR, and average MREG BOLD signal

During BH, the etCO$_2$ trace reflected the atmospheric CO$_2$ level at the end of inspiration and verified successful task performance in the included datasets (Figure 2(a)). HR continuously decreased during BH but quickly recuperated to NV level (Figure 2(b)).

NIRS signals showed elevations of HbO and HbT, marking increased CBF towards the end of BH that prevailed after BH. In contrast, HbR showed only a small increase after BH that levels in contrast to HbO and HbT (Figure 2(c)).

The mean MREG signal showed a classical BOLD-like signal increase after the BH onset. The mean MREG signal peaked 10–13 s after BH, depending on the selected IC ROI (Figure 2(d)).

The frontal DMN MREG and frontal NIRS HbT and HbO signals showed similar time courses. Notably, in contrast to the NIRS signals, the MREG signals showed oscillations at the beginning of BH.

### BH effect on cerebral cardiovascular pulsation amplitude

Cardiac-filtered NIBP data showed an initial drop that reached the baseline level after 10 s, remained for 10 s and then dropped reaching a pressure minimum at the end of BH period (Figure 2(e)). The MREG pulsation amplitude data from anterior cerebral artery (Figure 2(f)) resembled the NIBP curve (post hoc temporal correlation $r = 0.84$, $p < 0.00001$). NIBP time course preceded that of MREG artery (post hoc cross-correlation applying MATLAB *xcorr*, temporal lag $= 1.1$ s). Cardiovascular amplitude of HbO signal presented small drops at the beginning of and following BH (Figure 2(g)). The cardiovascular amplitude of HbR signal remained stable during the BH challenge but elevated significantly after the end of BH (Figure 2(h)).

### Cardiovascular pulse amplitudes increase in respiratory centers

The MREG cardiovascular PtP envelope signals extracted from ICA ROIs covering brain stem ($p = 0.00002$, corrected), midbrain ($p = 0.001$, corrected), somatosensory cortex ($p = 0.00005$, corrected), sagittal sinus ($p = 0.003$, corrected) and visual ($p = 0.0057$, not corrected) showed significant amplitude elevations after BH (Figure 3). Default mode ROIs and CSF presented a tendency to slightly elevate amplitude, while white matter remained stable during BH (Supplementary Figure 2). The MREG amplitude elevation was in line with HbR amplitude increase detected in NIRS (Figure 2(h)). Surprisingly, brainstem and midbrain showed clearly biggest amplitude changes.

The most significantly increased cluster in the cardiovascular pulse amplitude map (z-score $> 5$, FWE-corrected $p < 0.05$) represents respiratory control areas in the brain. Importantly, clusters increased in amplitude, size, and amount with increasing number of performed BH runs (Figure 4(a), Table 1). In BH1–2, significant cluster occurred in the brainstem's ventral and dorsal respiratory control areas at upper and lower part of the pons. There, the spatial extent of the signal amplitude maxima was smallest in BH2 (Figure 4(b)). In BH3, the spatial distribution of the voxels diverged towards upper and dorsal parts of the brainstem. Finally, in BH4–5, an extension to brain peduncles, thalami, left hypothalamus, right caudate nucleus, and amygdalae was observed. Comparing pulse amplitude changes in those regions across BH runs, strongest elevations occurred immediately following the BH period, but temporal profiles varied between BH runs (Figure 4(b)). Most regions showed a spike at the start of BH period in BH5. Areas that have the most significant increases in the cardiovascular pulse amplitudes during BH are precisely located in the respiratory control areas of the human brain (Figure 4(d)).

### MREG cardiovascular impulse spread during BH

The spatiotemporal pattern of cardiovascular pulse presented significant changes over time, which initially
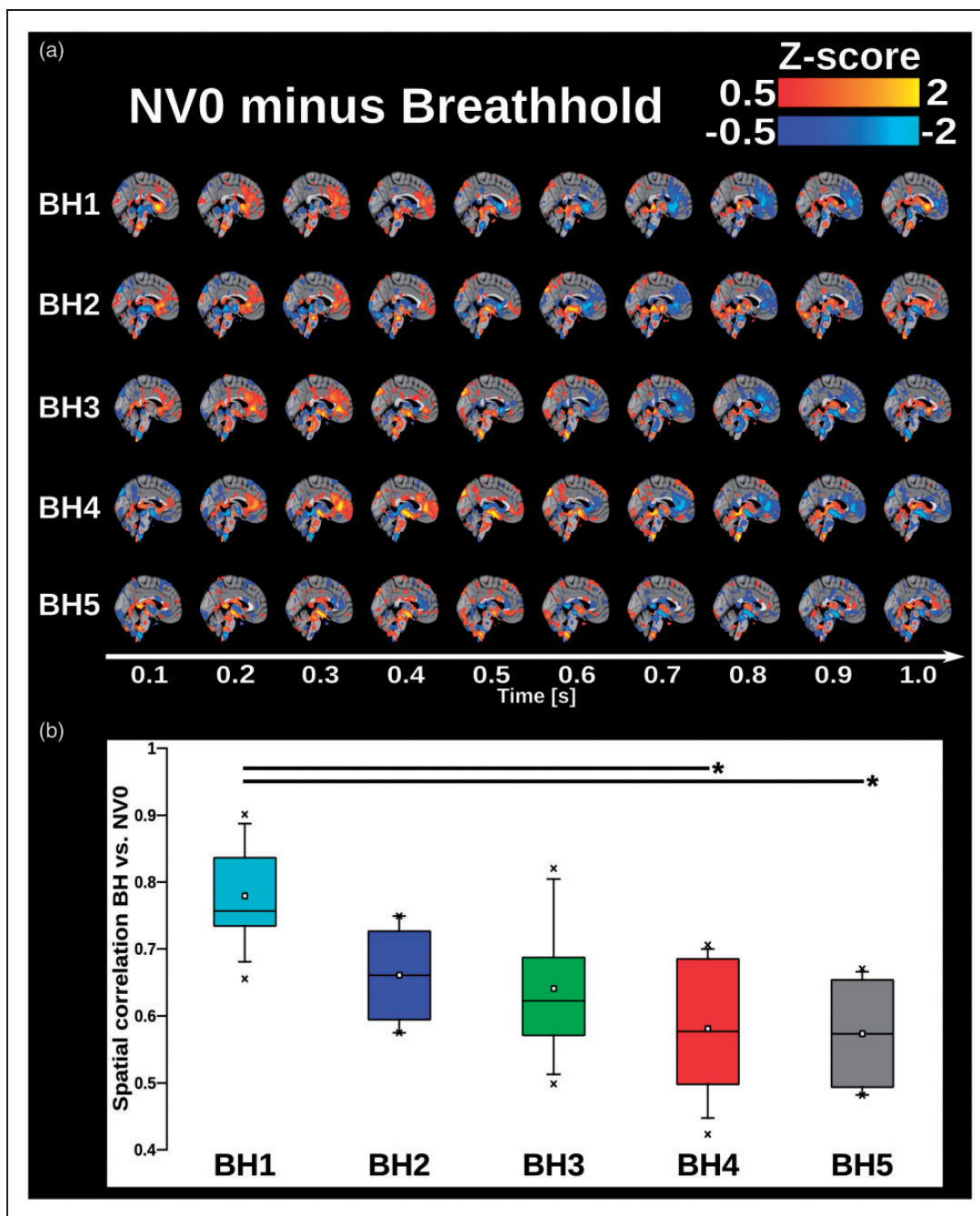
**Figure 5.** (a) 3D time lapsed group averaged and phase-matched differential QPP maps of cardiac pulsations of the human brain calculated by subtracting each BH run from NV0. Pulse represented in 1 s time frame with time steps of 0.1 s corresponding MREG TR. Red colors show areas where amplitude of NV0 is greater compared to BH and blue colors show areas where amplitude of BH is greater compared to NV0. (b) 4D spatial correlation of cardiovascular QPP map between BH1–5 and NV0 (colored boxes) On each box, the line and square indicate the median and mean, respectively, and the bottom and top edges of the box indicate the 25th and 75th percentiles, respectively. Whiskers extend to the 5th and 95th percentiles and minimum and maximum values are plotted as 'x'. Significance bars indicate a significant difference between respective BHs runs, with *: $p < 0.01$ and **$p < 0.001$, uncorrected (Supplementary Table 1).

dominated in the peri-arterial areas in BH1–2. However, with increasing number of BH runs, the differences between NV versus BH became stronger and more widespread and started to disseminate increasingly towards peripheral brain structures (Supplementary Figures 4 and 5). A phase shift in the pulse propagation occurred during BH5 (Figure 5(a)). Late BH runs showed a low spatial similarity with early

ones, indicating that the magnitude of pulse propagation change during BH exceeded normal alterations in cardiovascular pulse propagation (Figure 5(b), Supplementary Table 3).

## Discussion

Our results replicated previously identified BH-induced increases in brain oxygenation levels (MREG BOLD and NIRS HbO) in cortical areas. Central blood pressure dropped at BH onset and end, and was highly correlated to arterial MREG signal pulse amplitude. Interestingly, the maximum cerebral cardiovascular pulse amplitude showed dynamically growing increases within the respiratory brain centers with each passing BH. Similarly, the spatial spread of the cardiovascular pulse wave became increasingly altered by each BH. The BH challenge did not entail significant alterations in cardiovascular pulsation amplitude in most of the cortical grey matter structures, neither in the white matter nor CSF. Frontal oxygenation pulse amplitude showed a tendency to drop following BH, but it was smaller and modulated in comparison to those seen in the arteries.

### BOLD signal and neurovascular responses during BH

Using MREG BOLD signal analysis, we observed an overall increase in signal intensity (Figure 2(d)), which matched those detected in earlier studies. After an initial drop, the BOLD has been shown to increase during BH due to vasodilation in the cortex.[8,10,11,45] We observed a slight initial signal decrease followed by a bigger increase towards the end of the BH period, which is consistent with studies employing a BH paradigm starting with inhalation.[46]

MREG cardiovascular pulse amplitude data indicated that BH induced small increases in the cortical ROI's and in the CSF (Supplementary Figure 2), similar to HbR in the cortex. Despite the mean arterial BP drop, the amplitudes increase in the cortex, mostly after BH. BH-induced increases in CBF have been confirmed by arterial spin labeling MR perfusion techniques[8] and transcranial doppler.[47] An increased CBF elevates oxy/deoxyhemoglobin concentration ratio, leading to increased BOLD signal change due to reduced de-phasing of the spins around vessels.[9] This effect has been explained by an increased washout of HbR due to vasodilation.[5,10,11,48]

The NIRS data revealed maximal HbO and HbT signal increases a few seconds after the cessation of BH (Figure 2(c)), which is in line with previous findings, employing a comparable length of BH periods.[20,49] HbO and HbT concentrations in primary motor area have shown a slight increase shortly after

the start of BH, the signals strongly decreased after 10 s of BH and peaked again 10 s after end of BH.[50] In our previous study, HBO and HbT signals in occipital cortex transiently decreased during the first 10 s of BH and followed a similar rising trend than observed in Figure 2(c) that exceeded baseline and peaked 10 s after end of BH while subjects were sitting.[32] Taken together, HbO and HbT signal peaks after BH are consistent observed across studies.

In contrast, HbR concentration did not decrease, as one might expect as a cause of the increase in BOLD signal. Instead, also HbR presented a small peak following BH (Figure 2(c)), coinciding with a BOLD signal increase (Figure 2(d)). The BOLD signal increases following BH were reflected in the increased HbT and HbO levels, pointing to a vasodilating effect underlying the BOLD signal increase.[49] The blood volume expansion may extend from arteries and capillaries into the venous compartment alike, as described in the balloon model in activation hyperemia.[48] Our results indicate an accumulative increase of HbT and HbO, since their values do not return to the baseline like the HbR does. This suggests an increase in CBV, which also may be linked to the detected changes in 3D cardiovascular pulse dynamics in Figure 5.

Another noteworthy finding was that in our experiment, the BH challenge induced a marked drop in blood pressure, which was reproduced in the envelope of cardiovascular pulse amplitude of MREG signal from an anterior cerebral artery (Figure 2(e) and (f)). This finding is of importance, since it verifies the accuracy of our multimodal neuroimaging data: two independent measures of blood flow (NIBP vs. MREG) showed virtually identical signals during BH challenge. The continuous NIBP time courses were also consistent with those observed in our pilot study.[32]

One would expect that since BOLD signal increases in the cortex, the cardiovascular pulsations should also increase due to vasodilation of vessels. Furthermore, the accompanying blood pressure drop during BH should increase cardiovascular brain pulse amplitude in frontobasal HbR (Figure 2(h)), MREG in cerebral grey matter, and white matter/CSF (Figure 3 and Supplementary Figure 2). However, the cardiovascular amplitude increases were significant only in brain stem, midbrain, SM1 and sagittal sinus. Surprisingly, cardiovascular pulsations remained relatively stable throughout the cortical grey and white matter. In the deep structures, especially in the brain stem, the amplitude changes were much larger. Along these lines, BH induced a continuous decrease in HR that recuperated during subsequent resting free ventilation, which once more confirmed results of the pilot study.[32] Due to unfirm fingertip attachment, finger movement, temperature, or other factors, the peripheral $SpO_2$ sensor

sometimes fails to monitor the HR changes and thus central measures like NIBP tend to be more reliable.

The increase in mean cardiovascular NIRS signal pulsation amplitude of HbO after end of BH (Figure 2(g)), seems to be consistent with other research which found that the amplitude of the arterial pulse wave of the cerebral microcirculation measured by NIRS increased following BH compared to preceding rest.[47]

## Cardiovascular pulse amplitude increased in respiratory control centers

Plotting the maximal increase of cardiovascular MREG signal pulse resulted in a map of the respiratory control network. The most interesting finding was that the repeated BH runs presented a dynamic increase in both amplitude of pulsations and size of the involved network towards latter BH runs. Notably, the results precisely mapped the respiratory control centers in the brainstem, including dorsal and ventral respiratory groups below the pons (medullary respiratory centers), the pre-Bötziger complex, as well as the pontine pneumotaxic and apneustic centers (Figure 4(d)). The respiratory control centers in the brainstem generate and regulate a rhythmic breathing pattern. In short, the respiratory rhythm arises in the pre-Bötzinger complex, the medullary centers control inspiratory muscles, and the pontine centers fine-tune smooth inspiration and expiration.[43]

It seems possible that the cardiovascular pulse amplitude peak observed in the respiratory control network is most likely caused by a vasodilation following neuronal activation within the control nuclei. The peak effect is combined with hypercapnia-induced $CO_2$ vasodilation effects, which seem to be very subtle based on our overall results in the brain. The spreading amplitude change from medullary and pontine nuclei into the thalamic areas showed dynamic adaptation of the respiratory network across BH runs (Figure 4(a)).

The amplitude changes also suggested that an increasing number of involved nuclei is most likely due to accumulation of $CO_2$. In BH1–2, the areas of increased cardiovascular pulse amplitude involved respiration control centers located in ventral medullar nuclei. In BH3–4, the previous pulsation area increased in size and returned towards areas in posterior medullar and up to pneumotaxic areas known to be activated by $CO_2$. In BH4–5, thalami, putamen, amygdalae, and hypothalamus showed increased pulse amplitude (Figure 4(a)).

Thalamic nuclei were shown to play an important role in integrating respiratory signals to and from the brainstem respiratory centers.[27] While cluster in pons, thalamus, and medulla have shown strong BOLD sensitivity to $CO_2$ stimulation, the anterior thalamus had strongest connectivity with amygdala, frontal cortex, and anterior cingulate cortex, which are areas mediating affective components of respiration.[27] Bilateral amygdala pulsation increase was maximal in BH4 towards the end of the BH paradigm, which may be explained by an effect of added discomfort due to repeated and relatively long 32 s breath-holds. Performing BH while lying in the MR scanner may additionally contribute to un-easiness and reduce well-being of the subjects.

Testing variants of chemo-stimulated breathing elicited by hypoxia, hypercapnia, and a combination of these stimuli, McKay et al.[25] observed increases in neural activity within regions of the brainstem, thalamus, striatum, cingulate cortex and cerebellum. Using a repeated BH paradigm, McKay et al.[24] revealed increased activity in areas commonly associated with response inhibition (insula, basal ganglia, frontal cortex, thalamus, amygdala, supramarginal gyrus, temporal gyrus), as well as superior dorsal and inferior ventral pons.[24] Their results were derived based on three brain volumes acquired during 15 s of BH and brainstem masking has been used. The current study stood to benefit from 10 Hz MREG sampling rate (yielding 320 brain volumes during 32 s of BH) at increased statistical power and yielded results corrected at the whole brain level per each BH separately. Nevertheless, despite the tremendous methodological differences, the concordance of the anatomical findings of the network with results by McKay[24,25] is striking. Thus, evidence from the current study corroborates the previously identified involvement of brainstem nuclei as well as midbrain areas responsible for respiratory control.

## Spatial impulse dynamics altered as a function of BH

In addition to the loci of maximal increase of cardiovascular MREG signal pulse, we furthermore investigated their intensity and spatiotemporal profiles and found differences between BH runs (Figures 4(b) and 5(a) and (b)). In line with our hypothesis that cardiovascular brain pulsations would change as a response to BH challenge, strongest amplitude elevations were detected immediately following the BH period.

The dynamic respiratory nuclei responses can be explained by individual physiological adaptation mechanisms, as nuclei in pons and midbrain are coupled to cardiorespiratory changes. For example, physiological changes have been shown to correlate with focal brainstem activity in slow breathing and hypoxic challenges.[26] Moreover, the anatomical spread of the cardiovascular pulse within the brain was altered as a function of BH in a similar way to the respiratory center amplitude change (Figure 5(a)). As more

brainstem nuclei became involved, the cardiovascular pulse propagation also became increasingly different when compared to pulses in normoventilation suggesting accompanying vasomotor tone changes (Figure 5(b)).

Both increasing involvement of $CO_2$ sensing nuclei and altered pulse spread changes during repeated BHs can be connected to accumulation. The accumulating $CO_2$ is most likely related to the increased blood flow and volume seen in the NIRS as non-leveling HbT and HbO after BH. The altered involvement of the respiratory control nuclei may also further modulate vasomotor centers and thus induce widespread changes that then manifest as significant alterations in the cardiac pulse spread in the brain. Moreover, the amplitude of the pulses within the nuclei tended to increase as a function of the BH.

### Relevance of brain pulsation mapping

Importantly, to precisely describe disease-related changes in the cardiac pulsations driving the glymphatic system, the method used to reveal these effects should be both spatially accurate and temporally sensitive in mapping most subtle changes in these pulsations. Our results showed that MREG data are both spatially and temporally highly accurate in detecting subtle alterations as it enabled mapping of dynamic effects in respiratory brainstem nuclei. The spatial spreading pattern of the pulse may convey significant information of physiological and pathological pulsation alterations, as a significant deviation may originate from altered glymphatic mechanisms or other hydrodynamic changes of the brain tissue.[4,51] Thus, the present study introduced valuable methods, which are promising to disclose aberrant glymphatic flow mechanisms and their (dys-)regulation in neurological diseases like dementia.

### Limitations

Recent ultra-fast fMRI inverse imaging techniques[52,53] such as MREG[2], generalized inverse imaging,[54] and echo-volumar imaging[55] enable critical signal sampling at least at 5 Hz without aliasing. Nevertheless, spin or gradient EPI MRI scanning techniques are still more commonly used. These sequences gather 3D brain volumes in 0.7–3 s via interleaved acquisition of slices to avoid slice spin excitation cross talk, which comes with the disadvantage of mixing the spreading signal change patterns and aliasing. Compared to acquiring subsequent slices several hundred ms apart in a jerking way of the interleaved sampling, ultra-fast MRI techniques capture the spreading pulse in a continuous manner.

The subjects decided freely whether to perform BH after inspiration or expiration, which warrants caution. However, based on low $EtCO_2$ during BH and the early increase in HbO, it seems likely that most subjects inspired upon start of BH. After screening of $CO_2$ data, we excluded data from two subjects completely as well as some sporadic flawed BHs (Supplementary Table 1), which underlines the necessity of proper $CO_2$ measurement. Masks monitoring gas composition during respiration would have enabled precise $CO_2$ and $O_2$ control, but breathing rhythm and entailed neuronal responses are nevertheless subject-specific. To account for effects of endexpiratory pressure on cortical oxygenation[50], valsalva maneuvers should be added in future studies. We assumed that the motivation to perform the BH challenge was equally high for all subjects. However, differences in previous experience with being an MR subject as well as affective responses to hypercapnia are likely to have influenced each subject's performance.[45] The long hypocapnia blocks might have elicited brain activation associated with air hunger.

The findings may be limited by the relatively low number of included subjects but given that MREG yielded 1000 whole-brain images per each BH run, we were able to follow the brain signals at a very high temporal precision that allows for a more accurate temporal separation of neuronal events and thereby increased statistical power.

The results speak of the high sensitivity of the MREG, since the brainstem is susceptible to respiratory CSF pulsations that mask activation tasks and often necessitate analysis to be masked only into brainstem voxels due to lack of statistical power. Intriguingly, the respiratory center mapping was based on detecting one *single* most significant pulse increase per voxel at group level >5 SDs, which speaks of high temporal sensitivity.

## Conclusions

This study set out to characterize the effects of repeated BH runs on cardiovascular pulsations of the human brain at high temporal resolution. This is the first time that dynamic increases in cardiovascular brain pulsations have been detected with in respiratory centers of the brain induced by repeated BHs. Importantly, the results show that the MREG data were both spatially accurate and temporally sensitive in the detection of alterations in the adaptability of the brain to breath-holding. Both increases and decreases of pulsation with high spatiotemporal accuracy matched physiological monitoring data. Furthermore, novel changes in anatomical spread of the pulse cycle were detected in the brain tissue during BH even in the absence of marked

pulse amplitude changes. The findings prove that MREG scanning offers a valuable tool for assessing brain status with respect to changes in physiological brain pulsations.

### Declaration of conflicting interests

The author(s) declared no potential conflicts of interest with respect to the research, authorship, and/or publication of this article.

### Authors' contributions

VKi, VKo designed the study, VKo, HH, TM, NH, VR, JK, AR, VKi collected and LR, VKo, TH, AZ, VB, VKi analyzed the data and LR, VKo, NH, VR, HH, JK, AR, TH, AZ, TM, VB, VKi wrote the manuscript.

### Supplementary material

Supplementary material for this paper can be found at the journal website: http://journals.sagepub.com/home/jcb

### ORCID iD

Lauri Raitamaa (ID) http://orcid.org/0000-0003-2884-6510
Janne Kananen (ID) http://orcid.org/0000-0001-6831-8056

### References

1. Biswal B, Zerrin Yetkin F, Haughton VM, et al. Functional connectivity in the motor cortex of resting human brain using echo-planar MRI. *Magn Reson Med* 1995; 34: 537–541.
2. Assländer J, Zahneisen B, Hugger T, et al. Single shot whole brain imaging using spherical stack of spirals trajectories. *Neuroimage* 2013; 73: 59–70.
3. Kiviniemi V, Wang X, Korhonen V, et al. Ultra-fast magnetic resonance encephalography of physiological brain activity – glymphatic pulsation mechanisms? *J Cereb Blood Flow Metab* 2016; 36: 1033–1045.
4. Nedergaard M. Garbage truck of the brain. *Science* 2013; 340: 1529–1530.
5. Bandettini PA and Wong EC. A hypercapnia-based normalization method for improved spatial localization of human brain activation with fMRI. *NMR Biomed* 1997; 10: 197–203.
6. Kastrup A, Krüger G, Neumann-Haefelin T, et al. Assessment of cerebrovascular reactivity with functional magnetic resonance imaging: comparison of $CO_2$ and breath holding. *Magn Reson Imag* 2001; 19: 13–20.
7. Corfield DR, Murphy K, Josephs O, et al. Does hypercapnia-induced cerebral vasodilation modulate the hemodynamic response to neural activation? *Neuroimage* 2001; 13: 1207–1211.
8. Kastrup A, Li T-Q, Glover GH, et al. Cerebral blood flow-related signal changes during breath-holding. *Am J Neuroradiol* 1999; 20: 1233–1238.
9. Posse S, Kemna LJ, Elghahwagi B, et al. Effect of graded hypo- and hypercapnia on fMRI contrast in visual cortex: quantification of $T*2$ changes by multiecho EPI. *Magn Reson Med* 2001; 46: 264–271.
10. Wise RG, Ide K, Poulin MJ, et al. Resting fluctuations in arterial carbon dioxide induce significant low frequency variations in BOLD signal. *Neuroimage* 2004; 21: 1652–1664.
11. Murphy K, Harris AD and Wise RG. Robustly measuring vascular reactivity differences with breath-hold: normalising stimulus-evoked and resting state BOLD fMRI data. *Neuroimage* 2011; 54: 369–379.
12. Di X, Kannurpatti SS, Rypma B, et al. Calibrating BOLD fMRI activations with neurovascular and anatomical constraints. *Cereb Cortex* 2013; 23: 255–263.
13. Lipp I, Murphy K, Caseras X, et al. Agreement and repeatability of vascular reactivity estimates based on a breath-hold task and a resting state scan. *Neuroimage* 2015; 113: 387–396.
14. Biswal B, Hudetz AG, Yetkin FZ, et al. Hypercapnia reversibly suppresses low-frequency fluctuations in the human motor cortex during rest using echo–planar MRI. *J Cereb Blood Flow Metab* 1997; 17: 301–308.
15. Birn RM, Cox RW and Bandettini PA. Experimental designs and processing strategies for fMRI studies involving overt verbal responses. *Neuroimage* 2004; 23: 1046–1058.
16. Birn RM, Murphy K, Handwerker DA, et al. fMRI in the presence of task-correlated breathing variations. *Neuroimage* 2009; 47: 1092–1104.
17. Stillman AE, Hu X and Jerosch-Herold M. Functional MRI of brain during breath holding at 4 T. *Magn Reson Imag* 1995; 13: 893–897.
18. Kastrup A, Li T-Q, Takahashi A, et al. Functional magnetic resonance imaging of regional cerebral blood oxygenation changes during breath holding. *Stroke* 1998; 29: 2641–2645.
19. Holper L, Scholkmann F and Seifritz E. Time–frequency dynamics of the sum of intra- and extracerebral hemodynamic functional connectivity during resting-state and respiratory challenges assessed by multimodal functional near-infrared spectroscopy. *Neuroimage* 2015; 120: 481–492.
20. Molinari F, Liboni W, Grippi G, et al. Relationship between oxygen supply and cerebral blood flow assessed by transcranial Doppler and near – infrared spectroscopy in healthy subjects during breath – holding. *J Neuro Eng Rehab* 2006; 3: 16.
21. Parkes MJ. Breath-holding and its breakpoint. *Exp Physiol* 2006; 91: 1–15.

22. Holper L, Scholkmann F and Seifritz E. Prefrontal hemo-dynamic after-effects caused by rebreathing may predict affective states – A multimodal functional near-infrared spectroscopy study. *Brain Imag Behav* 2017; 11: 461–472.

23. Homma I and Masaoka Y. Breathing rhythms and emotions. *Exp Physiol* 2008; 93: 1011–1021.

24. McKay LC, Adams L, Frackowiak RSJ, et al. A bilateral cortico-bulbar network associated with breath holding in humans, determined by functional magnetic resonance imaging. *Neuroimage* 2008; 40: 1824–1832.

25. McKay LC, Critchley HD, Murphy K, et al. Sub-cortical and brainstem sites associated with chemo-stimulated increases in ventilation in humans. *Neuroimage* 2010; 49: 2526–2535.

26. Critchley HD, Nicotra A, Chiesa PA, et al. Slow breath-ing and hypoxic challenge: cardiorespiratory conse-quences and their central neural substrates. *PLoS One* 2015; 10: e0127082.

27. Pattinson KTS, Mitsis GD, Harvey AK, et al. Determination of the human brainstem respiratory con-trol network and its cortical connections in vivo using functional and structural imaging. *Neuroimage* 2009; 44: 295–305.

28. Korhonen V, Hiltunen T, Myllylä T, et al. Synchronous multiscale neuroimaging environment for critically sampled physiological analysis of brain function: hepta-scan concept. *Brain Connect* 2014; 4: 677–689.

29. Hugger T, Zahneisen B, LeVan P, et al. Fast under-sampled functional magnetic resonance imaging using nonlinear regularized parallel image reconstruction. *PLoS One* 2011; 6: e28822.

30. Myllylä TS, Elseoud AA, Sorvoja HSS, et al. Fibre optic sensor for non-invasive monitoring of blood pressure during MRI scanning. *J Biophotonics* 2011; 4: 98–107.

31. Gesche H, Grosskurth D, Küchler G, et al. Continuous blood pressure measurement by using the pulse transit time: comparison to a cuff-based method. *Eur J Appl Physiol* 2012; 112: 309–315.

32. Myllylä T, Zacharias N, Korhonen V, et al. Multimodal brain imaging with magnetoencephalography: a method for measuring blood pressure and cardiorespiratory oscil-lations. *Sci Rep* 2017; 7: 172.

33. Myllylä T, Korhonen V, Suraźyński Ł, et al. Measurement of cerebral blood flow and metabolism using high power light-emitting diodes. *Measurement* 2014; 58: 387–393.

34. Sorvoja HSS, Myllylä TS, Kirillin MY, et al. Non-invasive, MRI-compatible fibreoptic device for functional near-IR reflectometry of human brain. *Quantum Electron* 2010; 40: 1067–1073.

35. Huppert TJ, Diamond SG, Franceschini MA, et al. HomER: a review of time-series analysis methods for near-infrared spectroscopy of the brain. *Appl Opt* 2009; 48: D280–D298.

36. Jenkinson M, Beckmann CF, Behrens TEJ, et al. FSL. *Neuroimage* 2012; 62: 782–790.

37. Beckmann C, Mackay C, Filippini N, et al. Group com-parison of resting-state FMRI data using multi-subject ICA and dual regression. *Neuroimage* 2009; 47: S148.

38. Filippini N, MacIntosh BJ, Hough MG, et al. Distinct patterns of brain activity in young carriers of the APOE-$\varepsilon$4 allele. *Proc Natl Acad Sci U S A* 2009; 106: 7209–7214.

39. Kiviniemi V, Starck T, Remes J, et al. Functional seg-mentation of the brain cortex using high model order group PICA. *Hum Brain Mapp* 2009; 30: 3865–3886.

40. Abou Elseoud A, Littow H, Remes J, et al. Group-ICA model order highlights patterns of functional brain con-nectivity. *Front Syst Neurosci* 2011; 5: 37.

41. Desikan RS, Ségonne F, Fischl B, et al. An automated labeling system for subdividing the human cerebral cortex on MRI scans into gyral based regions of interest. *Neuroimage* 2006; 31: 968–980.

42. Neurosynth, http://neurosynth.org/ (accessed 15 March 2018).

43. Majeed W, Magnuson M, Hasenkamp W, et al. Spatiotemporal dynamics of low frequency BOLD fluc-tuations in rats and humans. *Neuroimage* 2011; 54: 1140–1150.

44. Sherwood L. *Fundamentals of human physiology*, 4th ed. Belmont, CA: Brooks Cole, 2011.

45. Bright MG and Murphy K. Reliable quantification of BOLD fMRI cerebrovascular reactivity despite poor breath-hold performance. *Neuroimage* 2013; 83: 559–568.

46. Magon S, Basso G, Farace P, et al. Reproducibility of BOLD signal change induced by breath holding. *Neuroimage* 2009; 45: 702–712.

47. Viola S, Viola P, Litterio P, et al. Correlation between the arterial pulse wave of the cerebral microcirculation and CBF during breath holding and hyperventilation in human. *Clin Neurophysiol* 2012; 123: 1931–1936.

48. Buxton RB, Wong EC and Frank LR. Dynamics of blood flow and oxygenation changes during brain activa-tion: the balloon model. *Magn Reson Med* 1998; 39: 855–864.

49. MacIntosh BJ, Klassen LM and Menon RS. Transient hemodynamics during a breath hold challenge in a two part functional imaging study with simultaneous near-infrared spectroscopy in adult humans. *Neuroimage* 2003; 20: 1246–1252.

50. Knauth M, Heldmann M, Münte TF, et al. Valsalva-induced elevation of intracranial pressure selectively decouples deoxygenated hemoglobin concentration from neuronal activation and functional brain imaging cap-ability. *Neuroimage* 2017; 162: 151–161.

51. Xie L, Kang H, Xu Q, et al. Sleep drives metabolite clear-ance from the adult brain. *Science* 2013; 342: 373–377.

52. Lin F-H, Wald LL, Ahlfors SP, et al. Dynamic magnetic resonance inverse imaging of human brain function. *Magn Reson Med* 2006; 56: 787–802.

53. Lin F-H, Tsai KWK, Chu Y-H, et al. Ultrafast inverse imaging techniques for fMRI. *Neuroimage* 2012; 62: 699–705.

54. Boyacioğlu R and Barth M. Generalized iNverse imaging (GIN): ultrafast fMRI with physiological noise correc-tion. *Magn Reson Med* 2013; 70: 962–971.

55. Posse S, Ackley E, Mutihac R, et al. High-speed real-time resting-state FMRI using multi-slab echo-volumar ima-ging. *Front Hum Neurosci* 2013; 7: 479.